The Generation of Warm Dense Matter Using a Magnetic Anvil Cell

P.-A. Gourdain, A. B. Sefkow, and C. E. Seyler

***Abstract*— Warm dense matter is present at the heart of gas giants and large exo-planets. Yet, its most basic properties are unknown, limiting our understanding of planetary formation and evolution. In this state, where pressure climbs above 1 Mbar, matter is strongly coupled and quantum degenerate. This combination invalidates most theories capable of predicting the equation of state, the viscosity, or heat conductivity of the material. When such properties are missing, understanding planetary evolution becomes an arduous endeavor. Henceforth, research in this field is actively growing, using high-power laser or heavy ion beams to produce samples dense enough to overcome the 1-Mbar limit. These samples are not actively confined and tend to expand rapidly, precluding the existence of any thermodynamically stable equilibrium. However, a mega-ampere-class pulsed-power generator can produce confined matter in the Mbar range, providing two conditions are being met. First, the sample needs to be compressed cylindrically, to maximize magnetic pressure (compared to slab compression). Second, an "electrical damper" must be used to limit the formation of a plasma at the sample surface. This corona robs the main sample from valuable current and limits the homogeneity of the compression. According to numerical simulations, the setup proposed here, called a magnetic anvil cell (MAC), can reach pressures on the order of 1 Mbar using a mega-ampere pulsed-power driver. These samples span several millimeters in length. Unlike diamond anvil cell, the MAC has virtually no pressure limit. Furthermore, the current heats the sample to several eV, a temperature well beyond the capabilities of diamond anvil cells.**

***Index Terms*— Diamond anvil cell, pulsed-power generator, warm dense matter (WDM), Z-pinch.**

I. Introduction

THIS paper presents numerical simulations that demonstrate how pulsed-power drivers can generate large samples of warm dense matter (WDM), using a setup called a magnetic anvil cell (MAC). By "large," we mean on the order of the material grain size, or larger, i.e., mesoscale. WDM can be found in the core of giant planets, at the surface of brown dwarves, or at early times in inertial fusion experiments. It is a state of matter where ions are strongly coupled and electrons are partially degenerate. While being simultaneously in a plasma state and a condensed matter state, both plasma and condensed matter theories are unable to capture its basic properties. Going back to first principles and using density functional theory would prove impractical to model macroscopic systems. When dealing with planetary formation or fusion experiments, macroscopic conservation laws (e.g., MHD) are the only practical approach to numerical simulations. But they do require accurate models for the equation of state and transport coefficients such as viscosity, heat, or electrical conductivities. To benchmark theories capable of capturing the microscopic properties of WDM at the macroscopic scale, experimentalists need to generate large (>1 mm) samples of WDM. At this size, the velocity shear or temperature gradients can be measured effectively using a bright X-ray light source. While pulsed-power drivers were first used to study WDM, they fell out of favor due to the excessive corona building around the sample and precluding homogeneous implosion. Experiments using kilojoule lasers and heavy ion beams have been successful so far, but have some drawbacks: small sample size and bulk matter not completely at equilibrium. The sample size is limited by the amount of available energy. The lack of confinement precludes materials studies on time scale long enough to allow for proper equilibrium (e.g., strain redistribution). The MAC was designed to mitigate both limitations. This configuration compresses matter with a pulsed-power driver. As in the diamond anvil cell, an "electrical damper" is necessary to compress the central sample homogenously. This damper limits the formation of instabilities. Ultimately, it acts as a mechanical damper since it controls the amount of current that flows at the sample surface. At 1-MA, pressures as large as 2 Mbar can be obtained. Unlike diamond anvil cell, which pressure is limited by materials strength, the MAC has virtually no pressure limit. The damper material can be a metal, an insulator, or a preionized gas. We study here how the density and resistivity of the damper impact the quality of the implosion and the pressure of the central sample. After this introduction, this paper lists the basic elements of the MAC. Then, 2-D numerical simulations show the dynamics expected in the MAC. Finally, we look at the impact of damper mass density and electrical resistivity on the properties and the quality of the final WDM sample.

Manuscript received January 12, 2018; revised March 23, 2018; accepted April 14, 2018. Date of publication October 16, 2018; date of current version November 8, 2018. The review of this paper was arranged by Senior Editor F. Beg. *(Corresponding author: P.-A.Gourdain.)*

P.-A. Gourdain is with the Extreme State Physics Laboratory, Physics and Astronomy Department, University of Rochester, Rochester, NY 14627 USA, and also with the Laboratory for Laser Energetics, University of Rochester, Rochester, NY 14627 USA (e-mail: gourdain@pas.rochester.edu).

A. B. Sefkow is with the Laboratory for Laser Energetics, University of Rochester, Rochester, NY 14627 USA, and also with the Mechanical Engineering Department, University of Rochester, Rochester, NY 14627 USA.

C. E. Seyler is with the Laboratory for Plasma Studies, Cornell University, Ithaca, NY 14850 USA.

Color versions of one or more of the figures in this paper are available online at http://ieeexplore.ieee.org.

Digital Object Identifier 10.1109/TPS.2018.2867361

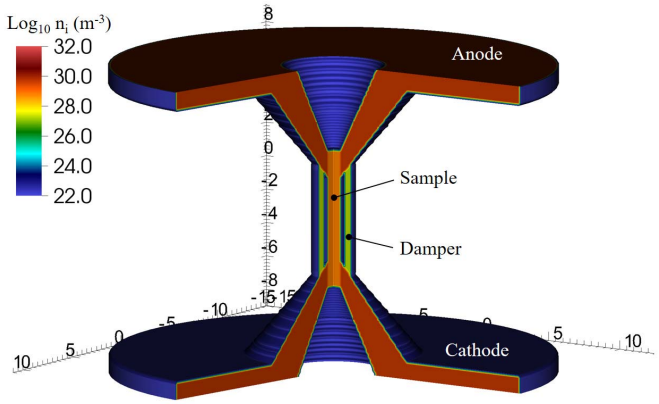

Fig. 1. 3-D view of the MAC. All distances are in millimeter. The anode and cathode have the density of copper-tungsten. The sample is made out of aluminum. The damper has variable density, given in the text.

II. Initial Conditions

The experimental setup is shown in Fig. 1. The MAC is composed of two cylinders. The innermost cylinder will be compressed by the pulsed-power generator and will turn into a WDM state as the current of the generator increases. It has the properties of aluminum in our simulations. The outer cylinder is the damper. The initial density and resistivity correspond to a silica aerogel. The top and bottom electrodes are conical, allowing a smooth transition of current from the generator connections down to the much smaller load.

The damper fulfills three different functions. First, the damper precludes the formation of a corona (i.e., ablated plasma) around the central sample. This corona diverts part of the current away from the main sample. As the current flows inside the corona, the corona temperature increases and its resistivity decreases, leading to larger currents inside the corona. Ultimately, part of the energy delivered by the driver is used to heat the corona and does not compress the sample directly. Second, the damper is limiting the formation [1] of electrothermal instabilities [2] at the surface of the central sample. Finally, the density and the resistivity of the damper can be chosen to optimize the compression for a given current. For identical samples, a heavy damper will slow down the implosion and reduce the overall pressure on the central sample at peak current while a lighter damper will allow for higher pressures. If the damper resistivity is large, then most of the current flows inside the sample and generates a coronal plasma which is difficult to compress, leading to smaller stagnation pressures. Since large current densities can also generate electrothermal instabilities [3], the presence of the damper slows down their growth.

This paper looks at the impact of the density and resistivity of the damper on the pressure and overall quality of the implosion of the sample. We used the extended-MHD code PERSEUS [4] in cylindrical coordinates to simulate the MAC on a mega-ampere class pulsed-power generator like HADES [5]. HADES is a 250-GW pulsed power driver using linear transformer technology [6] to generate a current of 1 MA in less than 150 ns. The time evolution of the current is given as

$$I = I_{\text{peak}} \sin\left(\frac{\pi}{2}\frac{t}{t_r}\right) \exp\left(-\frac{t}{t_{\text{d}}}\right) \tag{1}$$

where I_{peak} is the peak current, t_{r} is the current rise time, and t_d is the current damping time [7]. While simulations have been performed in 2-D in this paper, Ref. [8] showed that 3-D instabilities are not detrimental to the overall compression of the sample. Therefore, this paper focuses on the impact of damper properties on sample compression ignoring 3-D instabilities. Clearly, these instabilities must be taken into account to truly define the parameter space that the MAC can cover for a 1-MA driver.

The simulation domain covers 15 mm horizontally and 18 mm vertically. The total number of cells is on the order of 60 000. The cell size is 70 μm. This resolution does not allow to estimate precisely the maximum pressure that can be reached in the proposed setup since the code cannot compress the rod beyond 70 μm. At stagnation, the maximum pressure can be computed from the equilibrium equation

$$\vec{\nabla} p = \vec{J} \times \vec{B}. \tag{2}$$

This equation gives a maximum pressure of 10 Mbar using 70 μm as the smallest allowed radius. Therefore, it is reasonable to infer that any pressure below 10 Mbar is realistically computed by the code.

III. Implosion Dynamics of the Magnetic Anvil Cell

First, we look at the implosion dynamics of the cell and show how it compares to the gas anvil cell previously published [8]. The simulation spanned 300 ns, with a current rise time t_r of 150 ns and a damping time of $6t_r$. In the case presented here, the damper is made from a foam, 30× lower than solid density (e.g., silica aerogel foam [9]).

Fig. 2 shows the simulation results for the central load region near current peak. Each panel is split into two plots. On the right side, the panel shows the ion density on the logarithmic scale. The left side gives the ion temperature, also on the logarithmic scale. At this stage, the damper has fully merged with the sample. The stagnation happens at 185 ns. At this time, the pressure is on the order of 2 Mbar. As a result, the maximum compression is reached due to driver (i.e., energy) limitation rather than the intrinsic limitation of the simulation resolution. By the time the implosion reaches stagnation, density spikes have formed around the dense column. The simulation shows three distinct locations where low-density spikes protrude outwards, indicating potential inhomogeneities in the compression of the sample.

Reducing the inhomogeneities caused by local instabilities is primordial to the success of the MAC. Radial inhomogeneities are perfectly acceptable if axisymmetry is enforced. Abel inversion techniques can be performed under these conditions. Therefore, even if the resolution of the simulation cannot resolve below 70 μm, any inhomogeneity along this direction does not pose a major problem. However, if viscosity measurements are to be successful, axial homogeneities are

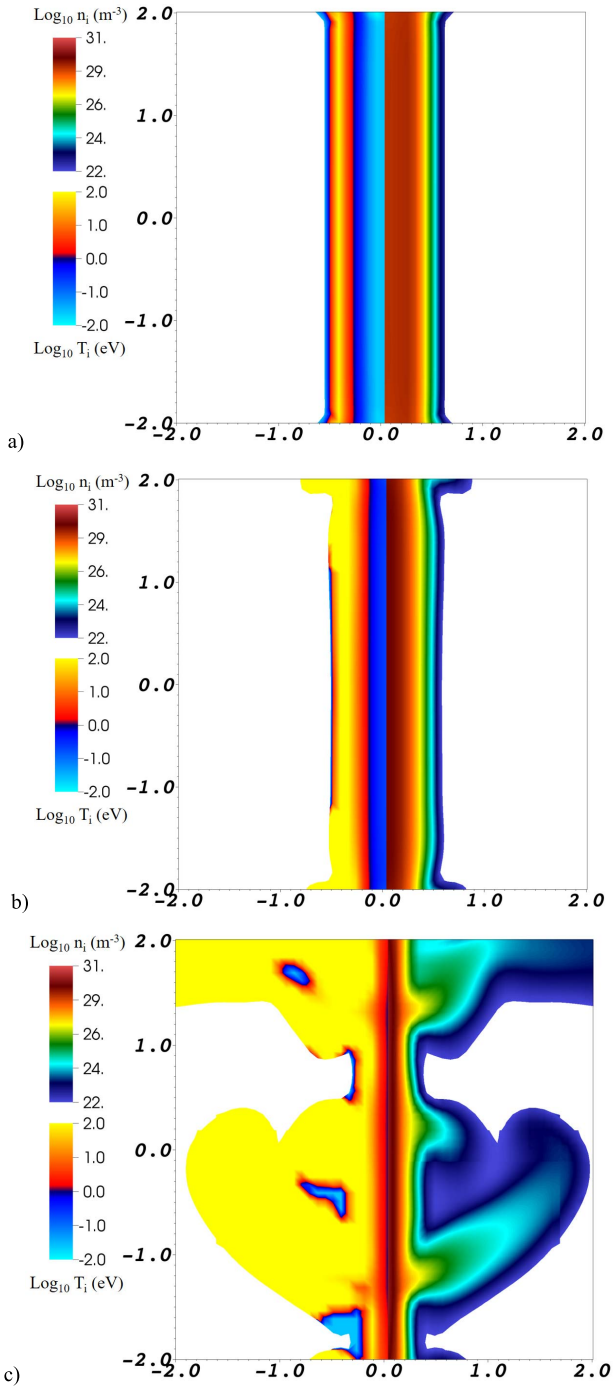

Fig. 2. Time evolution of the MAC for (a) $t = 140$ ns, (b) 160 ns, and (c) 180 ns. Each panel shows the ion density (right) and the ion temperature (left), plotted on the logarithmic scale. All dimensions are in millimeter. The regions were the ion density is smaller than 10^{22} m^{-3} are not plotted.

more problematic, since it is along this direction that the measurement will be most meaningful. We can quantitatively assess the impact of inhomogeneities on the pressure by plotting the ion temperature as a function of the ion density inside a chosen volume of the simulation domain. Fig. 3 shows the result of two collection volumes. When the collection volume is a hockey puck of 15 mm radius, spanning a height of 2 mm, with 1 mm above and 1 mm below the midplane, all the data points fall into a red circle. In this case, the variation

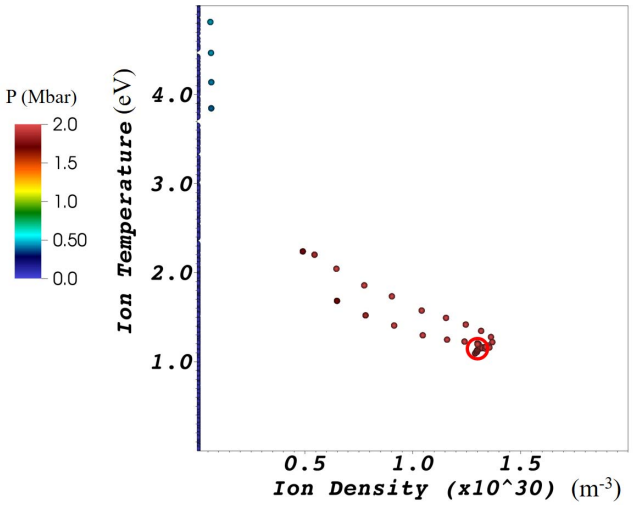

Fig. 3. Ion temperature versus ion density at $t = 180$ ns for a collection hockey puck encompassing 2 mm above and below the midplane, for a foam density 30× smaller than solid density. When the collection volume is limited to 1 mm above and below the midplane, we obtain the data points located inside the red circle.

in density is less than 10^{29} m^{-3} and 0.1 eV (or 10% for both), quite an acceptable variation. However, when we extend the collection volume to encompass the full actively compressed sample, i.e., 2 mm above and below the midplane, the data spread well outside of the red circle. There is an obvious dispersion of data points in this case, well above 100%. This simulation shows that only the central 2 mm of the sample can be used effectively. The maximum pressure is reached closest to the midplane, an indication that parasitic behavior associated with end effects will have a limited impact on the central region of the sample.

Overall, we have found that this axial dependence is relatively well bounded in the MAC proposed here. While higher resolutions or 3-D simulations may reveal inhomogeneities at smaller scales, the simulation presented here shows encouraging behavior at the 100 μm scale.

IV. Impact of the Foam Density

We now look at the implosion dynamics of the cell when the foam density is three times lower. All the other parameters are kept constant. In this case, we arrive at stagnation in 160 ns, 20 ns earlier than in the previous case. Fig. 4 shows that there is only a minor difference between the two cases. The data point spread and overall dynamics are very similar. This indicates that the mass of the damper weakly impacts the properties of the final sample. Regardless, a damper with much lower density would be difficult to manufacture and set in place experimentally. A much denser damper would start to interfere with the X-rays used to probe the properties of the sample in the WDM state. As a result, we found that the foam density of the silica aerogel (i.e., 1/30 solid density) is ideal.

V. Impact of the Foam Resistivity

After looking at the impact of the foam density, we turn to its resistivity. In the initial case shown in previous figures, the foam had a resistivity following a version of the

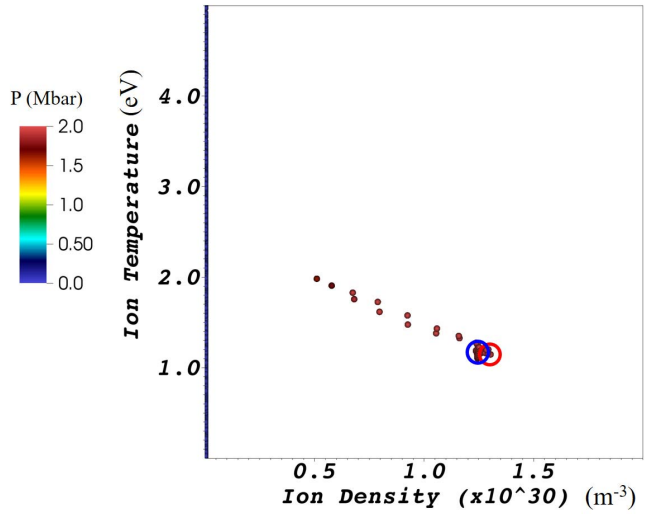

Fig. 4. Ion temperature versus ion density at $t = 180$ ns for a collection hockey puck encompassing 2 mm above and below the midplane, for a foam density 100× smaller than solid density. When the collection volume is limited to 1 mm above and below the midplane, we obtain the data points located inside the blue circle. The red circle from Fig. 3 is shown here for comparison.

Lee and More [10] and Desjarlais [11] resistivity specifically tailored for aluminum. We now artificially increase this resistivity by a factor of 10, 100, or 1000, compared to this reference resistivity ρ_{ref}. This increase takes place inside the damper only.

Fig. 5 shows the impact of the damper resistivity on the sample pressure at stagnation. As before, end effects start to be noticeable 1 mm above and below the midplane. However, they have a minor impact on the central region of the sample. What is more remarkable is the impact of the damper resistivity on the pressure itself. Paradoxically, as the resistivity increases and more current starts to flow inside the sample, the sample pressure diminishes at stagnation.

A similar effect was seen when a preionized gas puff was used [12]. When the current flows inside the sample, the formation of a corona is unavoidable early in the discharge. When the magnetic field is low, this corona heats up and partially shields the sample from the external magnetic field. The pressure also increases rapidly, and the plasma goes from high beta to low beta.

In the presence of a preionized gas puff, the current hardly flows inside the central sample at the beginning of the discharge. It only flows later, when the gas puff has fully imploded onto the sample and when the magnetic field surrounding the sample is already large. This large magnetic field prevents the ablated plasma from expanding and heating up. In this respect, the gas performs the function of a plasma opening switch.

A similar effect happens here. When the damper resistivity is high, the current flows mostly inside the sample, early in the discharge. Therefore, the formation of the corona happens under a weak magnetic field that cannot quench the formation and expansion of the corona. In fact, the remnants of the corona are still present at stagnation, visible to the right

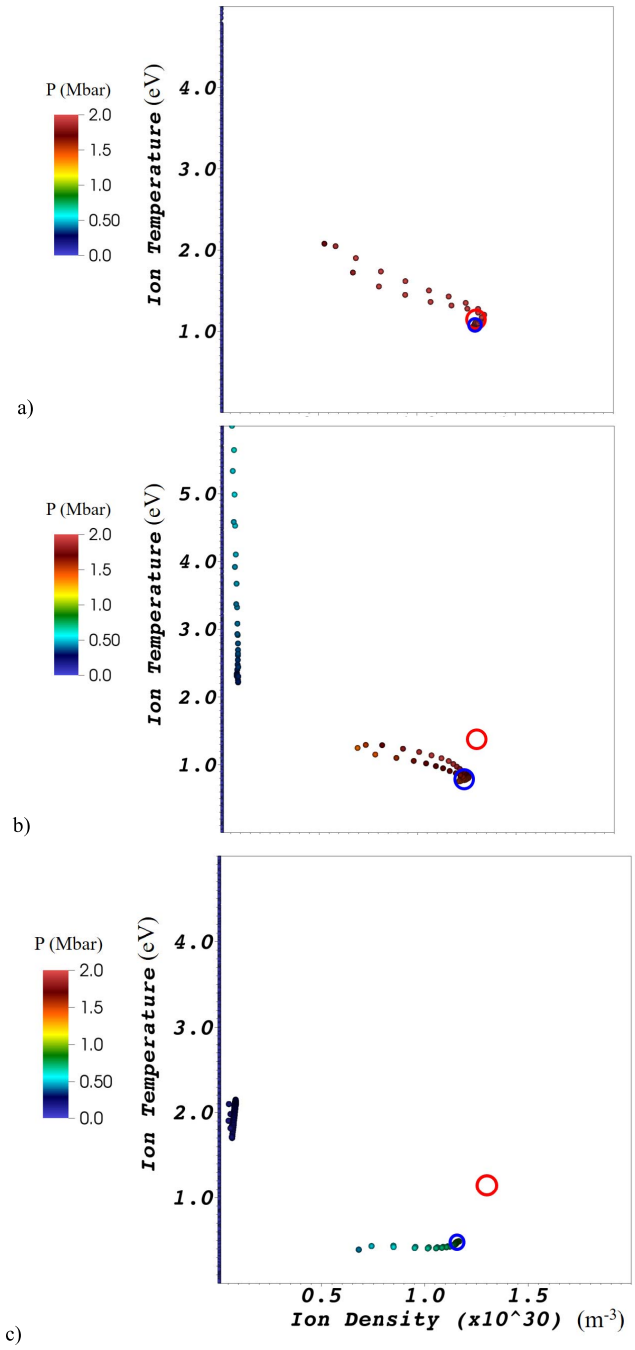

Fig. 5. Ion temperature versus ion density at $t = 180$ ns for a collection hockey puck encompassing 2 mm above and below the midplane, for a foam resistivity (a) 10×, (b) 100×, and (c) 1000× lower than the initial foam resistivity. When the collection volume is limited to 1 mm above and below the midplane, we obtain the data points inside the blue circle. The red circle from Fig. 3 is shown here for comparison.

of the vertical axis in Fig. 5(b) and (c). When the damper resistivity is low, a sizable portion of the current flows inside the damper, limiting the formation of the corona, which has now disappeared from Figs. 3, 4, and 5(a). The full current is forced back into the sample only when the damper has fully imploded onto the sample, ramming both corona and magnetic field into the sample. This process is more efficient and the effective pressure is higher, as shown in Fig. 5(b) and (c).

When the resistivity is kept low ($\rho \sim 10\rho_{\text{ref}}$), the stagnation pressure of the sample stays around 2 Mbar, mostly unchanged compared to the reference case. As the resistivity increases ($\rho \sim 100\rho_{\text{ref}}$ then $\rho \sim 1000\rho_{\text{ref}}$), there is more and more current flowing inside the sample and the pressure at stagnation is smaller, as just explained. This effect can give a extra degree of freedom, allowing to produce lower pressures using the same discharge current. The change in resistivity does not impact the quality of this implosion in the central region.

VI. Conclusion

This paper showed how a foam damper is an effective means to control and improve the compression of large scale cylindrical samples. The effect of the foam density is relatively weak on stagnation pressure. A change in foam resistivity impacts more dramatically the stagnation pressure. During the implosion, all the way to stagnation, the central region of the sample implodes relatively homogeneously and the pressure reaches 2 Mbar along 2 mm of the sample axis. The variations in ion density and temperature are found to be smaller than $\pm 10\%$. While further studies are required to assess the quality of the sample under megabar pressures, the MAC shows great promise in the study of materials under extreme pressures at the mesoscale.

References

[1] K. J. Peterson *et al.*, "Electrothermal instability mitigation by using thick dielectric coatings on magnetically imploded conductors," *Phys. Rev. Lett.*, vol. 112, no. 13, p. 135002, 2014.

[2] K. J. Peterson *et al.*, "Electrothermal instability growth in magnetically driven pulsed power liners," *Phys. Plasmas*, vol. 19, no. 9, p. 092701, 2012.

[3] I. Blesener, B. Kusse, K. Blesener, J. Greenly, and D. Hammer, "Ablation and precursor formation in copper wire-array and liner *Z*-pinches," *IEEE Trans. Plasma Sci.*, vol. 40, no. 12, pp. 3313–3318, Dec. 2012.

[4] C. E. Seyler and M. R. Martin, "Relaxation model for extended magnetohydrodynamics: Comparison to magnetohydrodynamics for dense *Z*-pinches," *Phys. Plasmas*, vol. 18, no. 1, p. 012703, 2011.

[5] P.-A. Gourdain, M. Evans, B. Foy, D. Mager, R. McBride, and R. Spielman. (2017) "HADES: A high amperage driver for extreme states." [Online]. Available: https://arxiv.org/abs/1705.04411

[6] A. A. Kim *et al.*, "Development and tests of fast 1-MA linear transformer driver stages," *Phys. Rev. Accel. Beams*, vol. 12, no. 5, p. 050402, 2009.

[7] M. G. Mazarakis *et al.*, "High current, 0.5-MA, fast, 100-ns, linear transformer driver experiments," *Phys. Rev. Accel. Beams*, vol. 12, no. 5, p. 050401, 2009.

[8] P.-A. Gourdain and C. E. Seyler, "The impact of three dimensional MHD instabilities on the generation of warm dense matter using a MA-class linear transformer driver," *High Energy Density Phys.*, vol. 24, pp. 50–55, Sep. 2017.

[9] K. Falk *et al.*, "Temperature measurements of shocked silica aerogel foam," *Phys. Rev. E, Stat. Phys. Plasmas Fluids Relat. Interdiscip. Top.*, vol. 90, no. 3, p. 033107, 2014.

[10] Y. T. Lee and R. M. More, "An electron conductivity model for dense plasmas," *Phys. Fluids*, vol. 27, no. 5, p. 1273, 1984.

[11] M. P. Desjarlais, "Practical improvements to the lee-more conductivity near the metal-insulator transition," *Contr. Plasma Phys.*, vol. 41, nos. 2–3, pp. 267–270, 2001.

[12] P.-A. Gourdain, "The generation of warm dense matter samples using fast magnetic compression," *IEEE Trans. Plasma Sci.*, vol. 43, no. 8, pp. 2547–2552, Aug. 2015.

Authors' photographs and biographies not available at the time of publication.